



Numerical Modelling of NACA 0015 Airfoil Under the Erosion Condition

Pemodelan Numerik Airfoil NACA 0015 Dalam Kondisi Erosi

Rayhan Fariansyah Billad¹, James Julian^{1*}, Fitri Wahyuni¹, Waridho Iskandar² dan Nely Toding Bunga²

¹Mechanical Engineering, Universitas Pembangunan Nasional Veteran Jakarta, Jawa Barat 12450, Indonesia

²Fluid Mechanics Laboratory, Universitas Indonesia, Kampus Baru UI, Depok 16424, Jawa Barat, Indonesia

³Program Studi Teknik Mesin, Fakultas Teknik, Universitas Pancasila, Jakarta 12640, Indonesia

Article information:

Received:
24/11/2023
Revised:
01/12/2023
Accepted:
07/12/2023

Abstract

Airfoil that experiences erosion caused by flying debris that hit the airfoil can affect the performance of the airfoil. This research was studied to determine the effect of erosion with varying erosion length using numerical methods on the performance of the NACA 0015 airfoil. This research was simulated using the Computational Fluid Dynamics (CFD) approach. Reynolds Averaged Navier-Stokes (RANS) is implemented as the governing equation. The turbulence model used in this research is the k-epsilon model. The Reynolds number used is 1.5×10^6 . This research proves that the erosion effect can reduce the C_l value and increase the C_d value on the NACA 0015 airfoil. Increasing the erosion length on the airfoil can also affect the C_l value and C_d value, but this effect is insignificant. In the contour visualization, the airfoil that is experiencing erosion has a pressure contour that increases in the upper chamber and decreases in the lower chamber compared to the airfoil that does not experience erosion so that it can reduce the lifting force of the NACA 0015 airfoil. The flow velocity and streamline contours also show greater circulation in the erosion airfoil, which can accelerate the stall by 1° AoA. Then, variations in increasing erosion length on the airfoil do not show any significant differences in pressure contours or circulating flow.

Keywords: CFD, erosion, NACA 0015, erosion length, aerodynamics performance.

SDGs:



Abstrak

Airfoil yang mengalami erosi akibat partikel-partikel yang membentur airfoil dapat mempengaruhi performa airfoil. Penelitian ini dilakukan untuk mengetahui efek erosi tersebut dengan variasi panjang (*length*) erosi menggunakan metode numerik terhadap performa *airfoil* NACA 0015. Penelitian ini disimulasikan menggunakan pendekatan *Computational Fluid Dynamics* (CFD). *Reynolds Averaged Navier-Stokes* (RANS) diimplementasikan sebagai persamaan pengatur tersebut. Model turbulensi yang digunakan pada penelitian ini adalah model k-epsilon. Bilangan Reynolds yang digunakan yaitu 1.5×10^6 . Penelitian ini membuktikan bahwa efek erosi dapat menurunkan nilai C_l dan meningkatkan nilai C_d pada *airfoil* NACA 0015. Peningkatan panjang erosi pada *airfoil* juga dapat mempengaruhi nilai C_l dan nilai C_d , namun pengaruh tersebut tidak signifikan. Pada visualisasi kontur dapat terlihat bahwa *airfoil* yang mengalami erosi memiliki kontur tekanan yang lebih besar pada bagian *upper chamber* dan lebih kecil pada bagian *lower chamber* dibandingkan dengan *airfoil* yang tidak mengalami erosi, sehingga dapat mengurangi gaya angkat *airfoil* NACA 0015. Kontur kecepatan aliran dan *streamline* juga menunjukkan aliran bersirkulasi yang lebih besar pada *airfoil* erosi yang dapat mempercepat *stall* 1° AoA pada *airfoil* erosi. Kemudian, variasi peningkatan panjang erosi pada *airfoil* tidak menunjukkan adanya perbedaan yang signifikan pada kontur tekanan maupun aliran bersirkulasi.

Kata Kunci: CFD, erosi, NACA 0015, panjang erosi, performa aerodinamika.

*Correspondence Author
email : james@upnvj.ac.id



This work is licensed under a [Creative Commons Attribution-NonCommercial 4.0 International License](https://creativecommons.org/licenses/by-nc/4.0/)

1. INTRODUCTION

One of the most fundamental elements in human life is energy. However, with the increasing demand for energy, energy fulfillment has increased drastically, and fossil energy has become the most used energy these days (Omer, 2008). Due to the pollutants produced by fossil fuels, which is frequently used in industry or for commercial purposes, may damage the environment. Green energy, which can also be an environmentally advantageous alternative fuel, could become one of the alternatives. For instance, wind turbines, photovoltaics, geothermal power plants, and so on have a wide range of options for green energy applicants (Loutun *et al.*, 2021). There is an essential component on the blades of wind turbines called airfoil. The blades of wind turbines have an aerodynamic airfoil shape, which can increase the lift coefficient of the blades and convert the kinetic energy of the wind into mechanical energy on the blades (Li *et al.*, 2018). However, due to the unwanted debris in the sky, the blades could be damaged in every day of use. For instance, there may be erosion on the surface due to insects, sand particles, or birds that hit the blades. The erosion shape and dimension could vary and decrease the blade's performance (Wagner and Mathur, 2012).

Research on airfoils with various forms of damage to the airfoil surface has been widely carried out to determine the impact or effect of performance on the airfoil, like research conducted by Gharali *et al.* to determine the lift and drag coefficient under the impact of the erosion on the airfoil's leading edge with a Reynolds number of 1×10^6 and a reduced frequency (k) of 0.026. Variations in erosion thickness and length were investigated. The results showed that the most significant effect was shown for erosion thickness compared to erosion length. Variation of erosion with a thickness of 12% and a length of 14% has an average lift coefficient decrease of 17%, a thickness of 12% and a length of 4% has an average lift coefficient decrease of 20%, a thickness of 25% and a length of 14% has a decrease in lift coefficient an average of 34% (Gharali and

Johnson, 2012). Then, Wang *et al.* conducted CFD simulation research with varying pitting hole depths and Reynolds numbers. The results of this study show that the deeper the depth of the pitting hole causes a decrease in C_l/C_d , and the pitting hole has the greatest effect at an angle of attack of 8.1° , while it has a small effect when the angle of attack is smaller than 2.1° . When the pitting hole depth is below 0.5 mm, the aerodynamic performance of the S809 airfoil is more significantly affected by pitting erosion (Wang, Hu and Zheng, 2017). Another study was conducted by Sun *et al.* with semi-circular and cuboid erosion shapes on the leading edge of the airfoil with variations in depth of 0.3%c, 0.5%c, and 1%c. Erosion with a semi-circular shape and a depth of 0.3%c has the effect of decreasing C_l/C_d by 3.5% at AoA 8° , then decreases again at a depth of 0.5%c, and in the end, erosion with a depth of 1%c has a decrease in C_l/C_d of 26.3%. Cuboidal erosion significantly decreases C_l/C_d compared to semi-circular erosion at depths of 0.3%c and 0.5%c. However, at an erosion with depth of 1%c, the two forms of erosion tend to have insignificant differences in value (Sun *et al.*, 2023).

Information on the impact of erosion with respect to airfoil performance can be obtained from these studies by means of different erosion forms and types of airfoils. However, to understand more fully the effect of erosion on airfoil performance, there are a number of other things that can be investigated. This research, therefore, has been performed to identify additional effects of erosion with a change in the erosion length. This way, changes in airfoil performance with erosion under the influence of changes in the erosion length can be further understood. This research will be carried out on the NACA 0015 model airfoil using a CFD approach and the k-epsilon model. The position of the airfoil angle of attack varies between 0° to 25° AoA. Different variations of the erosion length are also applied with the values of 0.14c, 0.25c, and 0.40c of the airfoil chord (c). Through this study of varying the erosion length of NACA 0015 airfoil, it is hoped that knowing the effect of erosion and erosion length variations regarding the airfoil performances will be understood and applicable.

2. METHODOLOGY

2.1. Erosion

Erosion is the most common occurrence on wind turbine's airfoils. Particles in the air and insects colliding at the front edge of the airfoil are usually the cause of this phenomenon. This causes wear on the surface of the airfoil which, in turn, would lead to a rough and damaged leading edge that may reduce its overall performance (Wang, Hu and Zheng, 2017). In the context of this numerical study, we will have a specific focus on the main edge showing signs of erosion and which will be subject to major changes. This research will include a thorough examination to understand the performance differences with respect to baseline airfoils and eroded airfoils on top edge of NACA 0015 airfoil. The erosion model situated at the airfoil's leading edge has a thickness equal to 12% of the airfoil thickness ($tA/t = 0.12$) and length variations equivalent to 14%, 25%, and 40% of the airfoil chord ($hA/C = 0.14, 0.25, \text{ and } 0.40$).

2.2. Governing Equations

A numerical technique is employed to compute the airflow around the airfoil shape, which involves solving the steady-state equations known as the Reynolds Averaged Navier Stokes (RANS) equations. Equations (1) and (2) represent those equations. To generate a continuity equation for fluid flow, equation (1) and equation (2) will be used to formulate the momentum equation of fluid flow (Aftab and Ahmad, 2017). In the analysis of the flow direction, it is assumed that it occurs on the X axis.

$$\frac{\partial \rho}{\partial t} + \frac{\partial}{\partial x_i}(\rho u_i) = 0 \quad (1)$$

$$\frac{\partial}{\partial t}(\rho u_i) + \frac{\partial}{\partial x_i}(\rho u_i u_j) = -\frac{\partial p}{\partial x_i} + \frac{\partial}{\partial x_i} \left[\mu \left(\frac{\partial u_i}{\partial x_i} + \frac{\partial u_i}{\partial x_i} - \frac{2}{3} \delta_{ij} \frac{\partial u_i}{\partial x_i} \right) \right] + \frac{\partial}{\partial x_i}(-\rho x_i' u_i') \quad (2)$$

where:

- u_i, u_j = instantaneous velocity
- u_i', u_j' = velocity fluctuation
- x, x_i = spatial coordinates
- ρ = density of fluid
- p = pressure

δ_{ij} = Kronecker delta

t = time

Standard k-epsilon equations for modelling turbulence are used in this study. Due to its accuracy in delivering accurate results of turbulent flows characterised by medium to high Reynolds levels, this equation has been selected. To develop a turbulence model for this study, equations (3) and (4) are used. The transport equation for turbulence kinetic energy is defined by Equation 3, and the Specific Dissipative Rate equations are defined by equation (4) (Darbandi et al., 2006).

$$\frac{\partial(\rho k)}{\partial t} + \frac{\partial(\rho k u_i)}{\partial x_i} = -\rho u_i' u_j' \frac{\partial u_j}{\partial x_i} - \rho \epsilon + \frac{\partial}{\partial x_i} \left[\left(\mu + \frac{\mu_t}{\sigma_k} \right) \frac{\partial k}{\partial x_i} \right] + G_b \quad (3)$$

$$\frac{\partial(\rho \epsilon)}{\partial t} + \frac{\partial(\rho \epsilon u_i)}{\partial x_i} = C_{\epsilon 1} \frac{\epsilon}{k} \left(-\rho u_i' u_j' \frac{\partial u_j}{\partial x_i} + C_{\epsilon 3} G_b \right) - C_{\epsilon 2} \rho \frac{\epsilon^2}{k} + \frac{\partial}{\partial x_i} \left[\left(\mu + \frac{\mu_t}{\sigma_\epsilon} \right) \frac{\partial \epsilon}{\partial x_i} \right] \quad (4)$$

where:

u_i, u_j = instantaneous velocity

u_i', u_j' = velocity fluctuation

x, x_i = spatial coordinates

k = turbulent kinetic energy

ϵ = dissipation rate

μ = dynamic viscosity

μ_t = turbulence viscosity

σ_k = coefficient in turbulence models

$C_{\epsilon 1}, C_{\epsilon 2}, C_{\epsilon 3}$ = RANS model coefficients

G_b = turbulent kinetic energy production rate

ρ = density of fluid

p = pressure

t = time

2.3. Geometry

In this research, the chosen geometry is the NACA 0015 airfoil profile (Aziz et al., 2014). Specifically, four variations of this geometry will be utilized, the NACA 0015 baseline and the NACA 0015 erosion with three variations of the erosion model applied to the leading edge of the NACA 0015 airfoil. Figure 1 give a detailed description of these geometries. Before performing simulation on an altered geometry, baseline geometry is used to validate the data.

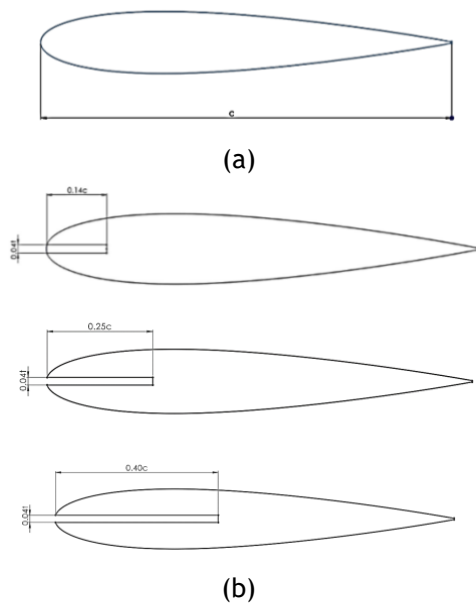


Figure 1. Airfoils of NACA 0015, (a) Baseline; (b) Erosion.

Both the NACA 0015 baseline and NACA 0015 erosion airfoils have a chord length (c) of 1000 mm. The erosion model on the leading edge of the airfoil, which will be the focus of the simulation, is characterized by a thickness equal to 0.04 times the airfoil thickness (t) and a length equivalent to 0.14, 0.25, and 0.40 of the airfoil chords (c).

2.4. Boundary Conditions

The boundary conditions of a fluid system serve to determine the boundaries of computational domain, replicating real-world experimental conditions in simulations. The domain is characterised by two distinct boundary conditions in this study, with the centre of a circular field lying at the trailing edge of an airfoil (Julian, Iskandar, Wahyuni and Ferdianto, 2022). The first part of the domain will be configured as a velocity inlet with the velocity of 21.9 m/s. The Reynolds number employed in this research is 1.5×10^6 . The outlet pressure, defined at a value of 0 Pa, is the second part of the boundary condition. In addition, the boundary conditions of the airfoil are designated as a barrier without slip. For a more detailed depiction of the boundary conditions, refer to Figure 2 which provides comprehensive dimensions and specifications.

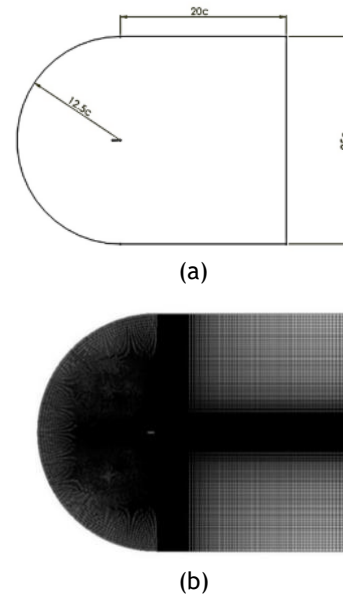


Figure 2. Boundary, (a) Boundary condition; (b) Boundary mesh.

2.5. Meshing

After geometry creation, the next step is meshing, in which a geometry is fragmented so that it can be composed of small elements to perform calculations (Sack and Urrutia, 2000). The mesh is made up of two main types of elements: quadrilateral and triangular. Structured mesh composed of quadrilateral elements has been selected for the purpose of this research. The choice of quadrilateral elements has been made on the basis that they provide a more precise meshing option with less error (Chen *et al.*, 2022). They also provide for smooth transitions between elements, which is what makes them a suitable choice for this study. Instead, mesh with triangular elements is more suitable for unstructured meshes that are used to create sophisticated geometrical configurations as a result of their flexibility when handling complicated geometries (Julian, Iskandar and Wahyuni, 2022). In this study, a separate mesh test will be carried out to identify the most efficient meshing strategy to perform subsequent simulations. The number of mesh elements will be varied for the purpose of testing, with the values of 50×10^3 , 75×10^3 , and 100×10^3 .

To achieve accurate and correct results in future simulations, this test will help identify the optimum mesh elements value. Figure 3 shows the meshing for both baseline airfoil and eroded airfoil.

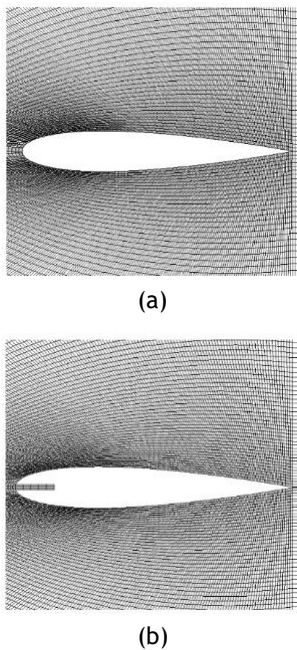


Figure 3. Meshing of the airfoils, (a) NACA 0015 Baseline mesh; (b) NACA 0015 Erosion mesh.

2.6. Aerodynamic of Airfoil

The examination of drag and lift forces is often part of the airfoil's aerodynamics. The drag force is an aerodynamic force which corresponds to the direction of the flow vector. In addition, if the vector is similar in direction to that of a fluid flow, lifting force may also be considered as an aerodynamic force. These forces are typically measured by dimensionless coefficients, called drag and lifting coefficients. Equations (5) and (6) provide the formulas used to calculate these coefficients (Julian, Iskandar, Wahyuni, Armansyah, et al., 2022).

$$C_d = \frac{2d}{\rho u^2 c} \tag{5}$$

$$C_l = \frac{2l}{\rho u^2 c} \tag{6}$$

where:

- C_d = coefficient of drag
- C_l = coefficient of lift
- d = drag force

- l = lift force
- ρ = density of fluid
- u = free-stream velocity
- c = chord length

3. RESULTS AND DISCUSSION

Mesh independence test in this research was checked to ensure convergence and the number of errors. There is a method called Richardson Extrapolation, which was generalized by Roache (Roache, 1994). In the mesh independence test that was carried out in this study, x component velocity values were taken into account at coordinates of $x=0.5$ and $y=0.15$. Mesh independence test will be performed in an order of 1.8, which corresponds to a ratio of variation 2 for the meshes. A safety factor of 1.25 will be used to test the mesh independently. For fine mesh and coarse mesh, the grid convergence index has been calculated as 1.100% and 2.4948% respectively. To conclude that the mesh variations are in the convergence index with the respective mesh errors of 0.8632%, 1.9568%, and 4.4359%, the final result of the mesh independence test is close to 1. Based on Figure 4, the fine mesh has values that are close to the parameters, so the mesh is used for further simulations.

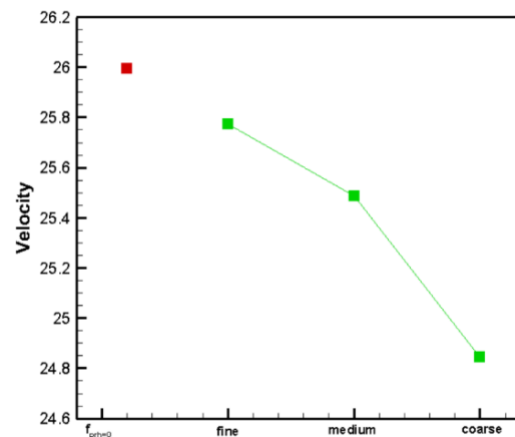
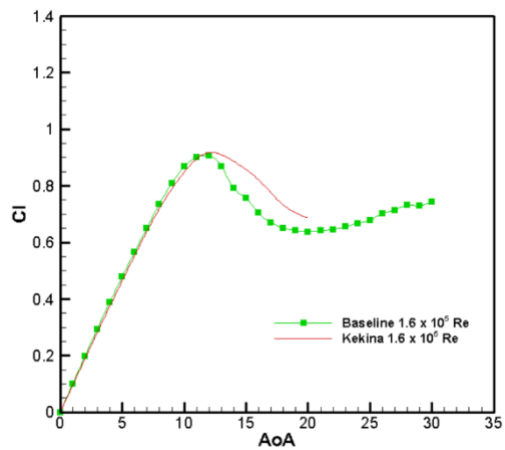


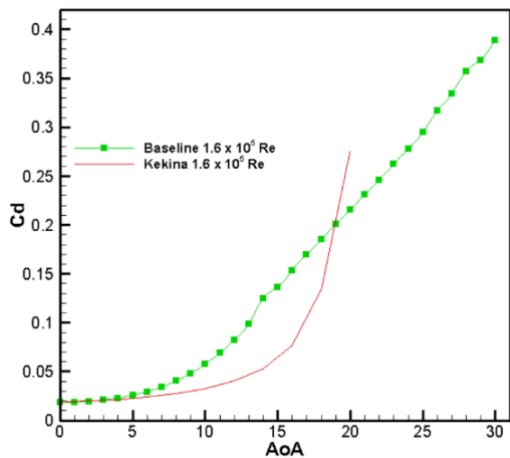
Figure 4. Mesh independence test result.

Validation in this research is done to ensure the simulation model has values close to the experimental results. Validation was carried out by comparing C_l and C_d NACA 0015 baseline data with data from experimental studies

conducted by Kekina and Suvanjumrat (Kekina and Suvanjumrat, 2017). Validation was compared at a Reynolds number of 1×10^6 . Figure 5a shows the comparison C_l results of CFD data and experimental data. In general, the trend pattern of all C_l curve data shows similarities. At an AoA of less than 10° , data between experiments and CFD show errors that tend to be smaller, whereas after AoA is more than 10° , there are errors that tend to be larger. This is caused by turbulence phenomena that are difficult to predict in the AoA. The graph of changes in C_d can be seen in Figure 5b. The experimental and CFD curves show similar data trends in changes in C_d towards AoA. The difference in C_d values between the baseline and experimental airfoils was not too significant when $\text{AoA} < 7^\circ$, but there was a significant difference after the AoA angle.



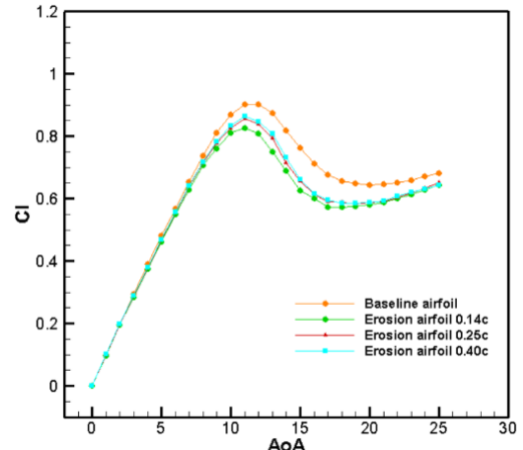
(a)



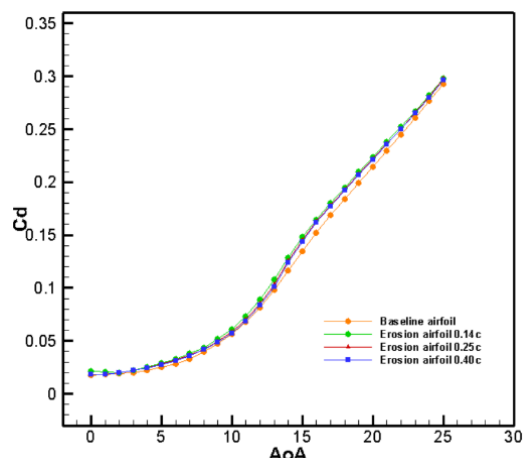
(b)

Figure 5. Airfoil validation, (a) C_l validation; (b) C_d validation.

The simulation results are shown in Figure 6a by comparing C_l values between the baseline and eroded airfoil with the length variations to show how it has worked out. Overall, the effect of erosion on airfoil's leading edge is similar in low AoA compared to baseline airfoil. However, the effect of erosion starts to affect the C_l value when the AoA is greater than 8° . The eroded airfoil stalls 1° faster compared to the baseline airfoil. The eroded airfoil stalls at $\text{AoA} 13^\circ$, while the baseline airfoil stalls at $\text{AoA} 14^\circ$. When the airfoil stalls, the C_l value tends to decrease further because the fluid flow circulates on the larger airfoil, which can reduce the C_l value of the airfoil. Variations in the erosion length also show a tendency to change the C_l value as the erosion length increases in the airfoil at $\text{AoA} > 9^\circ$ and $\text{AoA} < 20^\circ$, but it is not significantly different.



(a)



(b)

Figure 6. Velocity contour and streamlines, (a) C_l of the airfoils; (b) C_d of the airfoils.

The simulation results are shown in Figure 6b in the form of C_d values for variations in AoA and erosion length. The effect of erosion on the airfoil has been tested and proven to increase the C_d value of the NACA 0015 erosion airfoil. The erosion effect can increase flow separation, thereby increasing the C_d value of the airfoil. The flow separation in the upper chamber airfoil after the stall can also increase the C_d value, which is higher than before the stall occurred. The erosion length variations also do not affect the C_d value significantly.

Figure 7 provides a visual representation of fluid flow and velocity distribution around both the baseline NACA 0015 airfoil and the NACA 0015 erosion airfoil while also showing the variations in the erosion length. Visualization is carried out at AoA 15° by depicting speed and streamline contours. This visualization can make it easier for observers to see the phenomena around the airfoil. The image shows that an eroded airfoil significantly influences flow circulation compared to the baseline airfoil.

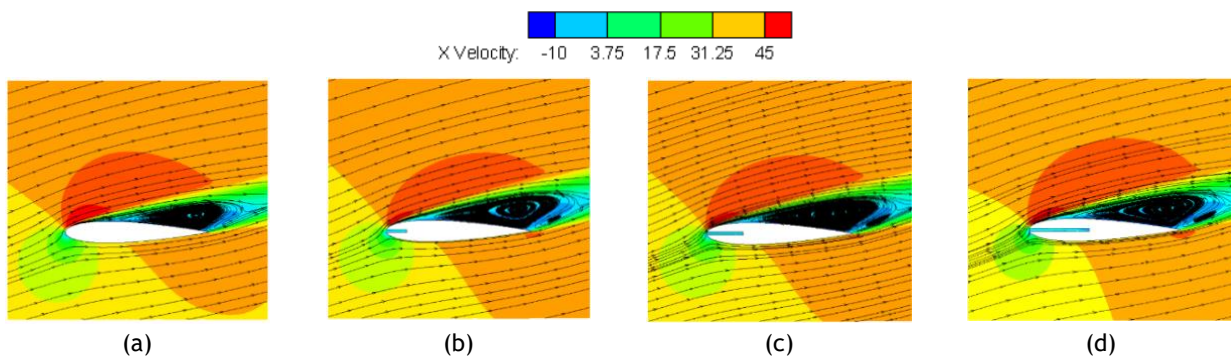


Figure 7. Velocity contour and streamlines, (a) Baseline AoA 15° Re 2.5×10^6 ; (b) Erosion 14%c AoA 15° Re 2.5×10^6 ; (c) Erosion 25%c AoA 15° Re 2.5×10^6 ; (d) Erosion 40%c AoA 15° Re 2.5×10^6 .

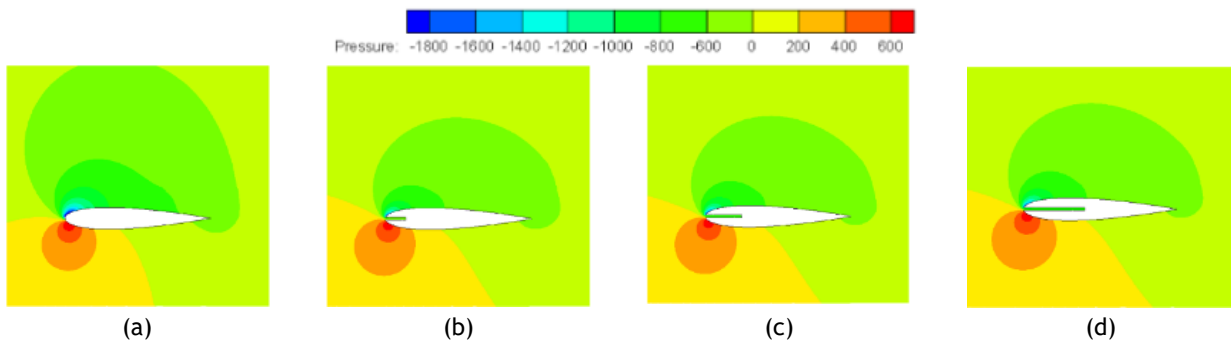


Figure 8. Pressure contour, (a) Baseline AoA 15° Re 2.5×10^6 ; (b) Erosion 14%c AoA 15° Re 2.5×10^6 ; (c) Erosion 25%c AoA 15° Re 2.5×10^6 ; (d) Erosion 40%c AoA 15° Re 2.5×10^6 .

The flow separation point in an eroded airfoil tends to be earlier than the baseline airfoil. The upper chamber of the erosion airfoil has a larger circulation compared to its baseline, and there is an additional flow from the trailing edge. The circulating flow, which tends to be greater, can have a stalling effect on eroded airfoil, which occurs faster than the baseline airfoil. Variations in the erosion length also affect the circulation

behavior of the airfoil, but it is not significantly different.

Figure 8 shows a visual representation of the pressure contours surrounding both the baseline NACA 0015 airfoil and the NACA 0015 erosion airfoil with the length variations. The contour visualization is carried out when the airfoil has an AoA of 15° . This image shows that the pressure contour on the airfoil is greater in the lower

chamber than in the upper chamber so that the pressure difference can exert a lift force on the airfoil. The effect of erosion is proven to reduce pressure in the lower chamber and increase pressure in the upper chamber of the airfoil. This phenomenon can be seen in changes in the pressure distribution in the airfoil section. Thus, this can cause the lifting force on the eroded airfoil to decrease. The pressure contour of the airfoil is only affected slightly by variations in erosion length. The pressure distribution on the airfoil with length variations is not that much different between those variations.

Compared to prior research, this research shows the aerodynamic performances of NACA 0015 airfoil with the variation of different erosion lengths to find out a deep understanding of the influence of erosion length respecting NACA 0015 airfoil. Three visual representations, such as pressure contour, velocity contour, and streamline contour are also provided in this research to give a clear visualization. Recirculation flow between baseline airfoil and eroded airfoil can be seen in the streamline contour in this research as an enhancement to prior research.

4. CONCLUSION

Erosion on the NACA 0015 airfoil has been proven to change the values compared to airfoils that do not experience erosion. Airfoils that experience erosion are proven to cause a decrease in C_l values and can increase C_d values compared to airfoils that do not experience erosion. Variations in the length of the erosion do not seem to influence the performance of the airfoil significantly. Furthermore, the aerodynamic phenomenon around the airfoils can be seen in the visualization of the airfoil's pressure, velocity, and streamline contours. Eroded airfoils tend to have greater circulation flow than baseline airfoils.

The eroded airfoil pressure contour also increases in the upper chamber and decreases in the lower chamber compared to the baseline airfoil. Then, the stall phenomenon in eroded airfoils occurs at 1° AoA faster than in airfoil that does not experience erosion. This can be caused

by flow separation occurring more quickly in eroded airfoil compared to the baseline airfoil. This research has summarized a review of the effect of erosion and erosion length variations in NACA 0015 airfoil.

This paper using more variations with not only the variations of erosion length but also variations in erosion thickness for a better understanding of the effect of those variations regarding the aerodynamic performances of NACA 0015 airfoil. Therefore, a comparison between erosion length and erosion thickness could help understand which one has a more significant influence on the performance of an airfoil.

REFERENCES

- Aftab, S.M.A. and Ahmad, K.A. (2017) 'CFD study on NACA 4415 airfoil implementing spherical and sinusoidal Tubercle Leading Edge', *PLOS ONE*, 12(8), p. e0183456. A
- Aziz, P.D.A. *et al.* (2014) 'A simulation study on airfoils using VAWT design for low wind speed application', in *2014 4th International Conference on Engineering Technology and Technopreneuship (ICE2T)*. *2014 4th International Conference on Engineering Technology and Technopreneuship (ICE2T)*, pp. 105-109.
- Chen, X. *et al.* (2022) 'An Improved Structured Mesh Generation Method Based on Physics-informed Neural Networks'. arXiv.
- Darbandi, M. *et al.* (2006) 'Modification of the Standard k-epsilon Turbulence Model for Multi-Element Airfoil Application Using Optimization Technique', in *24th AIAA Applied Aerodynamics Conference*. American Institute of Aeronautics and Astronautics (Fluid Dynamics and Co-located Conferences). pp. 1-12.
- Gharali, K. and Johnson, D.A. (2012) 'Numerical modeling of an S809 airfoil under dynamic stall, erosion and high reduced frequencies', *Applied Energy*, 93, pp. 45-52.
- Julian, J., Iskandar, W., Wahyuni, F. and Ferdianto, F. (2022) 'Computational Fluid Dynamics Analysis Based On The Fluid Flow Separation Point On The Upper Side Of The Naca 0015 Airfoil With The Coefficient Of

- Friction', *Media Mesin: Majalah Teknik Mesin*, 23(2), pp. 70-82.
- Julian, J., Iskandar, W., Wahyuni, F., Armansyah, A., et al. (2022) 'Effect of Single Slat and Double Slat on Aerodynamic Performance of NACA 4415', *International Journal of Marine Engineering Innovation and Research*, 7(2), pp. 93-100.
- Julian, J., Iskandar, W. and Wahyuni, F. (2022) 'Aerodynamics Improvement of NACA 0015 by Using Co-Flow Jet', *International Journal of Marine Engineering Innovation and Research*, 7(4), pp. 284-291.
- Kekina, P. and Suvanjumrat, C. (2017) 'A Comparative Study on Turbulence Models for Simulation of Flow Past NACA 0015 Airfoil Using OpenFOAM', *MATEC Web of Conferences*, 95, p. 12005.
- Li, D. et al. (2018) 'Effects of the particle Stokes number on wind turbine airfoil erosion', *Applied Mathematics and Mechanics*, 39(5), pp. 639-652.
- Loutun, M.J.T. et al. (2021) '2D CFD Simulation Study on the Performance of Various NACA Airfoils', *CFD Letters*, 13(4), pp. 38-50.
- Omer, A.M. (2008) 'Green energies and the environment', *Renewable and Sustainable Energy Reviews*, 12(7), pp. 1789-1821.
- Roache, P.J. (1994) 'Perspective: A Method for Uniform Reporting of Grid Refinement Studies', *Journal of Fluids Engineering*, 116(3), pp. 405-413.
- Sack, J.-R. and Urrutia, J. (2000) *Handbook of Computational Geometry*. North Holland: Elsevier. [Print].
- Sun, J. et al. (2023) 'Influence of blade maximum thickness on airfoil performance with varied leading edge erosion rate', *Frontiers in Energy Research*, 10, pp. 1-15.
- Wagner, H.-J. and Mathur, J. (2012) *Introduction to Wind Energy Systems: Basics, Technology and Operation*. 1st edn. Berlin: Springer Berlin, Heidelberg. [Print].
- Wang, Y., Hu, R. and Zheng, X. (2017) 'Aerodynamic Analysis of an Airfoil With Leading Edge Pitting Erosion', *Journal of Solar Energy Engineering*, 139(061002), pp. 1-11.

